



HAL
open science

Nanometer-Scale Resolution Achieved with Nonradiative Excitation

Lina Riachy, Dalia El Arawi, Rodolphe Jaffiol, Cyrille Vézy

► **To cite this version:**

Lina Riachy, Dalia El Arawi, Rodolphe Jaffiol, Cyrille Vézy. Nanometer-Scale Resolution Achieved with Nonradiative Excitation. ACS photonics, 2018, 5 (6), pp.2217-2224. 10.1021/acsp Photonics.8b00063 . hal-02363346

HAL Id: hal-02363346

<https://utt.hal.science/hal-02363346>

Submitted on 14 Nov 2019

HAL is a multi-disciplinary open access archive for the deposit and dissemination of scientific research documents, whether they are published or not. The documents may come from teaching and research institutions in France or abroad, or from public or private research centers.

L'archive ouverte pluridisciplinaire **HAL**, est destinée au dépôt et à la diffusion de documents scientifiques de niveau recherche, publiés ou non, émanant des établissements d'enseignement et de recherche français ou étrangers, des laboratoires publics ou privés.

Nanometre-scale resolution achieved with Nonradiative Excitation

Lina Riachy, Dalia El Arawi, Rodolphe Jaffiol, and Cyrille Vézé*

*Lumière Nanomatériaux Nanotechnologies, Institut Charles Delaunay, UMR CNRS 6281,
Université de Technologie de Troyes, 12 rue Marie Curie, CS 42060, 10004 Troyes cedex,
France.*

E-mail: cyrille.vezy@utt.fr

Phone: +33 (0) 3 51 59 11 55. Fax: +33 (0)3 25 71 84 56

Abstract

Nonradiative Excitation Fluorescence Microscopy (NEFM) is a promising technique allowing the observation of biological samples beyond the diffraction limit. By coating a substrate with an homogeneous monolayer of quantum dots (QDs), NEFM is achieved through a nonradiative energy transfer from QDs (donors) to dye molecules located in the sample (acceptors). The excitation depth of the sample is then given by the Förster radius, which corresponds to few nanometers above the surface. The powerful axial resolution of NEFM is highlighted by observing the adhesion of Giant Unilamellar Vesicles (GUVs) on strong interaction with coated surfaces. In this paper, we demonstrate that the QD-quenching level is valuable to calculate and map the distance between the membrane and the surface with a high precision along the optical axis. By tuning the electrostatic interactions between the membrane and the substrate, we have been able to measure a height displacement of ≈ 1 nm of the lipid membrane. The experimental results were discussed according to simulations, which take into account all the common forces appearing between lipid membranes and surfaces.

Keywords

Biophotonics, Förster Resonance Energy Transfer, Membrane, Nanoscopy

Förster Resonance Energy Transfer (FRET) is now a standard technique, widely employed in biophysics and biophotonics. FRET relies on a nonradiative energy transfer from excited donor molecules to acceptor molecules in their ground state. This energy transfer is efficient as long as the distance between the two molecules is less than 10 nm. FRET is usually considered as a nanoscale ruler with a broad area of applications that includes structural biology,¹ biosensing,^{2,3} binding measurement between molecules⁴ or structure of intermembrane junction.⁵ The signal obtained from FRET is typically examined by spectra, fluorescence pictures or by time-resolved investigations. In this paper, we propose an original imaging method, based on donor quenching analysis, to measure, with a nanoscale accuracy, distances involved in the adhesion of membranes on a surface.

Giant Unilamellar Vesicles (GUVs) are extensively used as biomimetic objects to explore and understand physical basis of cell adhesion^{6,7} and to test new imaging techniques.^{8,9} As membrane composition can be easily modified with several kinds of lipids wearing charges or specific functions, the vesicles spreading will change as their interactions with the substrate change. Different optical tools were proposed to observe and understand the adhesion of lipid membranes or cells. First, Reflection Interference Contrast Microscopy (RICM)¹⁰⁻¹³ and related improvements (dual wavelength,¹⁴ refined version of RICM theory⁹) or Fluorescence Interference Contrast (FLIC) microscopy^{5,15,16} allowed quantitative measurements of the membrane-surface distance. Second, microscopy techniques using evanescent wave and its new adaptations, such as normalised Total Internal Reflection Microscopy (nTIRFM)^{8,17} and variable-angle Total Internal Reflection Fluorescence Microscopy (vaTIRFM),¹⁸ are also well suited to observe and quantify the adhesion of living cells or GUVs near a wall. However, all these techniques do not allow the observation of membrane nanometric displacement, related to tiny modulations of the membrane/substrate interactions. This is mainly due to the axial resolution of these usual techniques, which is, on soft material at room temperature, at best

≈ 5 nm for RICM and 5-10 nm for fluorescent technique. To measure membrane/substrate interdistance with a nanometric accuracy, we have recently proposed an appealing alternative to interferometry or Total Internal Reflection, based on FRET. This nanoimaging technique is called Nonradiative Excitation Fluorescence Microscopy (NEFM).¹⁹ NEFM is based on the activation of glass coverslip with quantum dots (QDs). This was firstly achieved through the deposition of a thin layer of PMMA highly doped with QDs.¹⁹ However, PMMA dewetting occurred after few hours or less, and therefore long time observations were not possible anymore. Moreover, the QDs density in PMMA cannot be controlled properly. In order to overcome these limitations, glass coverslips were activated by adding a monolayer of CdSe/ZnS quantum dots (QDs) with a silanisation process.²⁰ To highlight the powerful axial resolution of NEFM and the benefits of this new substrate preparation, we observed GUV spreading on glass substrate coated with QDs, when adhesion is mediated by electrostatic interactions. To this end the QDs were surrounded by a positively charged polymer, Poly-L-Lysine (PLL), and membranes were labeled with a negatively charged dye (DiD). The excitation depth in NEFM is typically ≈ 10 nm at the vicinity of the surface. This corresponds to two times the Förster radius. According to the FRET theory and by recording both QDs-quenching and fluorescence induced by FRET, a distance map between the surface and the lipid membrane can be reconstructed according to a straightforward image analysis compared to others methods. For example, in RICM (even in dual-wave length RICM),^{14,21} all refractive index should be known to get quantitative informations. Moreover, the data processing is very complex. FLIC or intermembrane FRET methods^{5,15,16,22} also involved a complex data processing and the conversion from FRET efficiency to a distance is difficult. In contrast, with our method, the absolute distance in each pixel of the picture can be obtained easily.

In this paper, we exploit NEFM to study the adhesion of GUVs mainly driven by van der Waals attraction and electrostatic attraction or repulsion. By tuning the strength of electrostatic attraction on the membrane adhesion, we achieved a 1 nm axial resolution with NEFM.

This constitutes a major breakthrough in nanoimaging. Until now, only the recent publication about cryogenic single molecule localization microscopy offers a sub-nanometer optical resolution.²³ At the opposite, more popular techniques such as STED,²⁴ single molecule localization combined with supercritical angle²⁵⁻²⁷ or structured illumination²⁸ or MIET,²⁹ only reach a resolution ≈ 10 nm at best, at room temperature. NEFM enables to overcome the 10 nm resolution barrier mainly because nonradiative energy transfer occurs between 1 and 10 nm.

Results and discussion

Surface characterization

We characterized our QDs layer on glass coverslips by SEM. The Fig.1 presents a SEM picture of QDs bound on silicon wafer (SEM images on glass coverslips are similar in term of homogeneity, but less contrasted due to glass substrate). This picture indicates that only a monolayer of QDs was achieved at a large scale. Thus our new method of preparation allowed us to create a homogenous surface coated with QDs. According to Fig.1, the surface coverage is about 25 % with a density of QDs about 5000 QDs/ μm^2 . This high surface density gives rise to a homogenous photoluminescent signal within a diffraction limited spot (no blinking was observed). This point is crucial for quantitative analysis in NEFM (the measured fluorescence fluctuations should be induced only by distance changes between donor and acceptor and not by QDs blinking). To exploit FRET theory, the quantum yield (ϕ_D) of our surface has to be estimated. The quantum yield of QDs change drastically as a function of solvents or environment. ϕ_D is given by Eq 1 where k_r is the radiative decay rate and k_{nr} is the non-radiative decay rate of QDs excited state.

$$\phi_D = \frac{k_r}{k_r + k_{nr}} \tag{1}$$

Table 1: Values of k_r , τ and k_{nr} to calculate the quantum yield ϕ_D of QDs in toluene solution or deposited on a surface and surrounded with PLL

	k_r (ns^{-1})	τ (ns)	k_{nr} (ns^{-1})	ϕ_D
QDs in toluene solution	0.0478	16.7	0.012	0.8
QDs in water	0.0338	-	-	-
QDs monolayer surrounded with PLL at glass/water interface	0.0399	8	0.0851	0.32

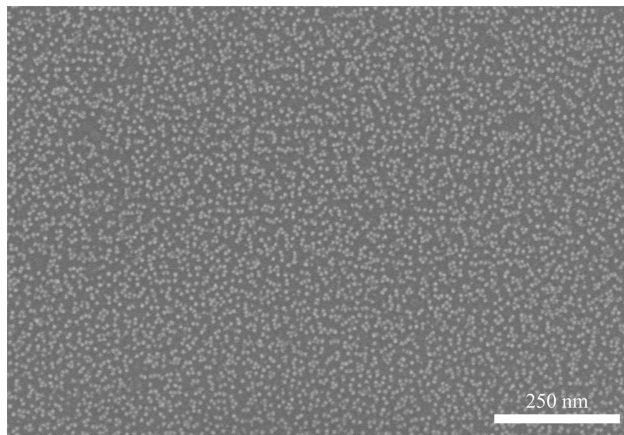


Figure 1: Typical SEM picture of surface coated with CdSe/ZnS QDs.

From the molar extinction spectra and emission spectra,³⁰ we estimated k_r for QDs in toluene by using the Strickler and Berg formula.³¹⁻³³ From this value, we have calculated k_r in water.³⁴ Then k_r is calculated for QDs monolayer at glass/water interface.³⁵ These results are shown in Table 1. Then k_{nr} is calculated by subtracting k_r from the value of the inverse of the measured fluorescence lifetime (τ) of QDs (Table 1). An example of lifetime measurements is presented in Fig.S1. We have determined the mean lifetime as proposed by A. I. Chizhik, I. Gregor, and J. Enderlein.³⁶ ϕ_D was estimated according to equation 1. $\phi_D \approx 0.32$ for our surface covered with QDs and with Poly-L-Lysin while $\phi_D \approx 0.8$ when QDs are in a toluene solution (as indicated by Sigma-Aldrich).

From QDs quenching and NEFM images to distance images

Calculation of R_0 , the Förster radius

The efficiency E_t of FRET process can be characterized according to:

$$E_t = \frac{1}{1 + \left(\frac{R}{R_0}\right)^6} = 1 - \frac{S_{D+A}}{S_D} \quad (2)$$

where R is the distance between donor and acceptor, R_0 is the Förster radius, S_D is the signal emitted by donors without acceptors and S_{D+A} , the signal emitted by donors when acceptors are added. To validate the relevance of equation 2 in our experiment, we have performed FRET experiments by controlling the distance between the QDs layer and a DiD layer. The FRET efficiency was then calculated and plotted as a function of the distance R (Fig S₂). These data can be fitted according to three different models : one acceptor coupled with one donor as depicted in equation 2, n acceptors coupled with one donor and a plane of acceptors coupled with one donor (see Supplementary information). From the obtained results, we have chosen the model when one acceptor is coupled with one donor. Then R_0^6 (in cm^6) need to be known and is calculated as following:

$$R_0^6 = \frac{9(\ln 10)\phi_D\kappa^2}{128\pi^5n^4N_a}J(\lambda) \quad (3)$$

with ϕ_D the quantum yield, N_a the Avogadro number, κ^2 the dipole orientation factor, n the refractive index of the medium (1.338 for glucose solution). The spectral overlap integral $J(\lambda)$ between donor and acceptor was numerically calculated according molar extinction and emission spectra (note that the maximum of DiD molar extinction coefficient is 210000 $\text{M}^{-1}\text{cm}^{-1}$ at 457 nm ³⁷). κ^2 is calculated from R. E. Dale, J. Eisinger, W. E. Blumberg.³⁸ DiD dipole orientation is perpendicular to the optical axis³⁹ and QDs dipole orientation is randomly distributed. Therefore, the angle between the DiD dipole and the axis defined by donors and acceptors is equal to $\pi/2$. Then $\kappa^2=1/3$. So the value of R_0 for our QDs surface

surrounded by Poly-L-Lysine at glass/water interface in interaction with a DiD layer is equal to 5.82 nm.

Quenching and fluorescence images

As vesicles contain sucrose (200 mM), and the surrounding medium is glucose at 250 mM vesicles gently settled on the Poly-L-Lysin/QDs surface due to gravitational force. When GUVs encounter the surface, lysis of all GUVs was observed in pure water due to the strong electrostatic attraction between the surface and GUVs.⁸ Therefore, only supported membranes are observed on the surface. As previously explained, the QDs layer is surrounded with Poly-L-Lysin in order to obtain positively charged surfaces. This charge depends on the salt concentration of the medium (Fig.S₃). At the opposite, the vesicles are labeled with DiD which is negatively charged. DiD charge does not change according to the salt concentration (as the pKa of the benzene sulfonic acid of DiD is at 2.54, and the pH working range in our experiments is higher than 6, the benzene sulfonic acid always exhibit a negative charge). Fig.2 shows a supported lipid bilayer on the surface observed i NEFM at 457 nm and TIRF at 633 nm. First, the TIRF illumination indicates the GUV lysis (no more vesicles were observed with defocusing imaging) (Fig. 2.a). Next, All experiments were performed with a laser irradiance of 50 mW/cm² at 457 nm and an acquisition time of 300 ms . At this irradiance, no direct excitation at 457 nm of the acceptor (DiD) is observed. As a consequence, the fluorescence emission of DiD (Fig.2b) is only due to FRET process.²⁰ In the spectral window of the QDs emission (Fig.2.c), quenching appears where DiD emission (Fig.2.b) is expected. Spectra recorded on QDs with and without supported lipid layer also confirms that FRET occurs (Fig.S₄). The fluorescence emitted by DiD through FRET is very homogenous without any fluctuation in time. Undulations of the membrane (related to Helfrich force) are suppressed due to the strong electrostatic attraction. Only photobleaching was observed with a slow decay rate (≈ 60 s). The Fig.3 presents a zoomed representation of our system. Due to the presence of octadecylamine ligands on the QDs, the PLL is deposited between

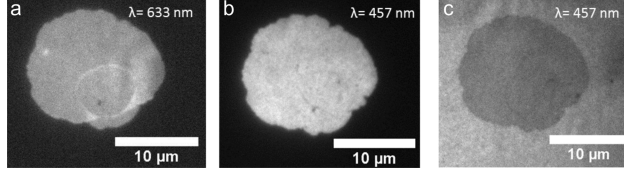


Figure 2: Lysis of vesicles on a QDs layer surrounded by Poly-L-Lysine. a: TIRF image at 633 nm. b: fluorescence emission of DiD excited at 457 nm (spectral detection window : 670-694 nm). c: photoluminescence of QDs excited at at 457 nm (spectral detection window : 490-610 nm).

the QDs, on the glass substrate, helped by electrostatic attraction between the amine groups of PLL and silanol groups on glass. Because it was diluted in a low concentration NaOH aqueous solution (i.e. poor solvent), in these conditions, PLL opted for a mushroom-like configuration as depicted in Fig.3. PLL hydrodynamic radius is about 5 nm in solution, so the thickness of PLL is similar or smaller than the QDs diameter.⁴⁰ Moreover the fluorescence observed on the lipid bilayer is laterally homogenous (Fig.2.b). This means that the lipid bilayer seems to be flat above the QD layer.

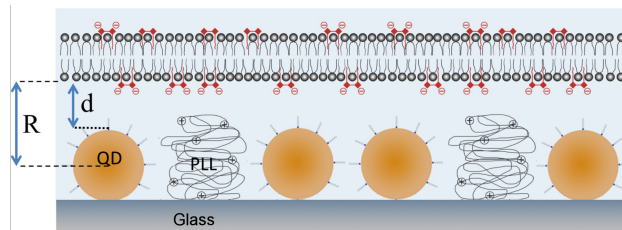


Figure 3: Schematic view of the studied system. R is the distance between the center of the QDs layer to the lipid membrane. d is the distance from the top of the QDs layer to the lipid membrane. d_0 is the corresponding equilibrium distance.

From the equation (2) and with image recorded through the detection spectral window of QDs, we have calculated the efficiency of FRET transfer, E_t , for each pixels. We used the NEFM image to determine on which pixel the transfer efficiency must be calculated because its contrast is very good. As a result, the fluorescence image is converted into a map of the normalized distance, denoted R/R_0 , between the surface and the membrane (Fig.4). From this map, we have also calculated the histogram of R/R_0 . The mean value ($\langle R/R_0 \rangle$) and

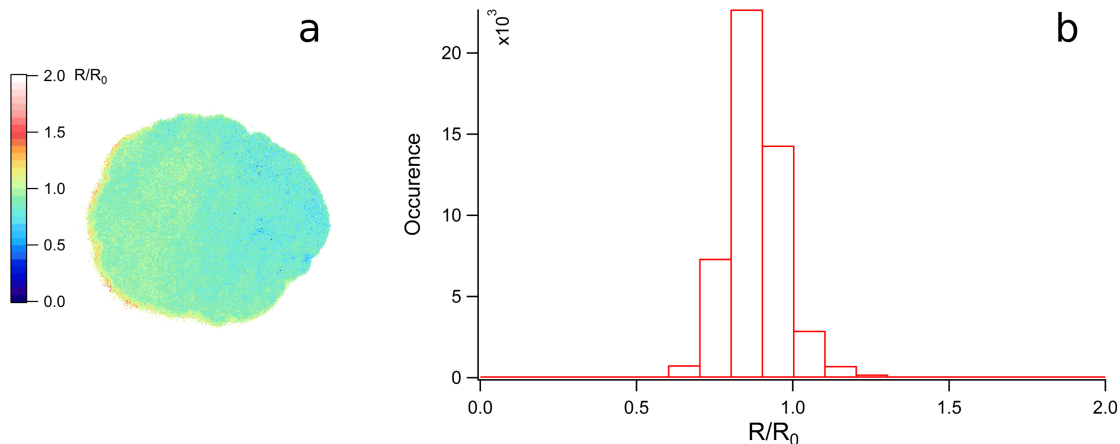


Figure 4: a. R/R_0 distance calculated from the data shown in Fig.3. b: Corresponding distance histogram.

the standard deviation (σ) were obtained according a Gaussian model. σ takes into account the height of the membrane fluctuation above the surface and also the heterogeneity of the functionalized surface. As shown in Fig.4, in pure water at pH=6, $\langle R/R_0 \rangle = 0.83$ and $\sigma = 0.003$. If we used the value previously calculated for $R_0 = 5.82$ nm, the mean distance $\langle R \rangle = 4.83$ nm \pm 0.02 nm. R corresponds to the distance from the center of the QDs to the lipid membrane. Therefore, the water gap thickness from the top of QDs to the membrane is ≈ 1 nm (the QDs radius is 4 nm as evaluated by SEM).

Influence of the addition of salt on the equilibrium distance d_0

In order to modulate the strength of the electrostatic attraction and measure how this modulation affects the equilibrium distance between the surface and the lipid bilayer, sodium hydroxide was added in the glucose solution. The salt concentration varied from 0 to 233 μ M. Below a concentration of 70 μ M, lysis of all vesicles is observed (Fig.5). On Fig.5 A₂, A₄, we observed the formation of a stack of lipid bilayers due to the presence of small vesicles inside bigger one. This can be easily checked on TIRF pictures recorded at 633 nm where brighter zones appear in the center. The fluorescence of the DiD is twice higher in the center. This is the signature of the presence of two lipid bilayers stacked in the center of

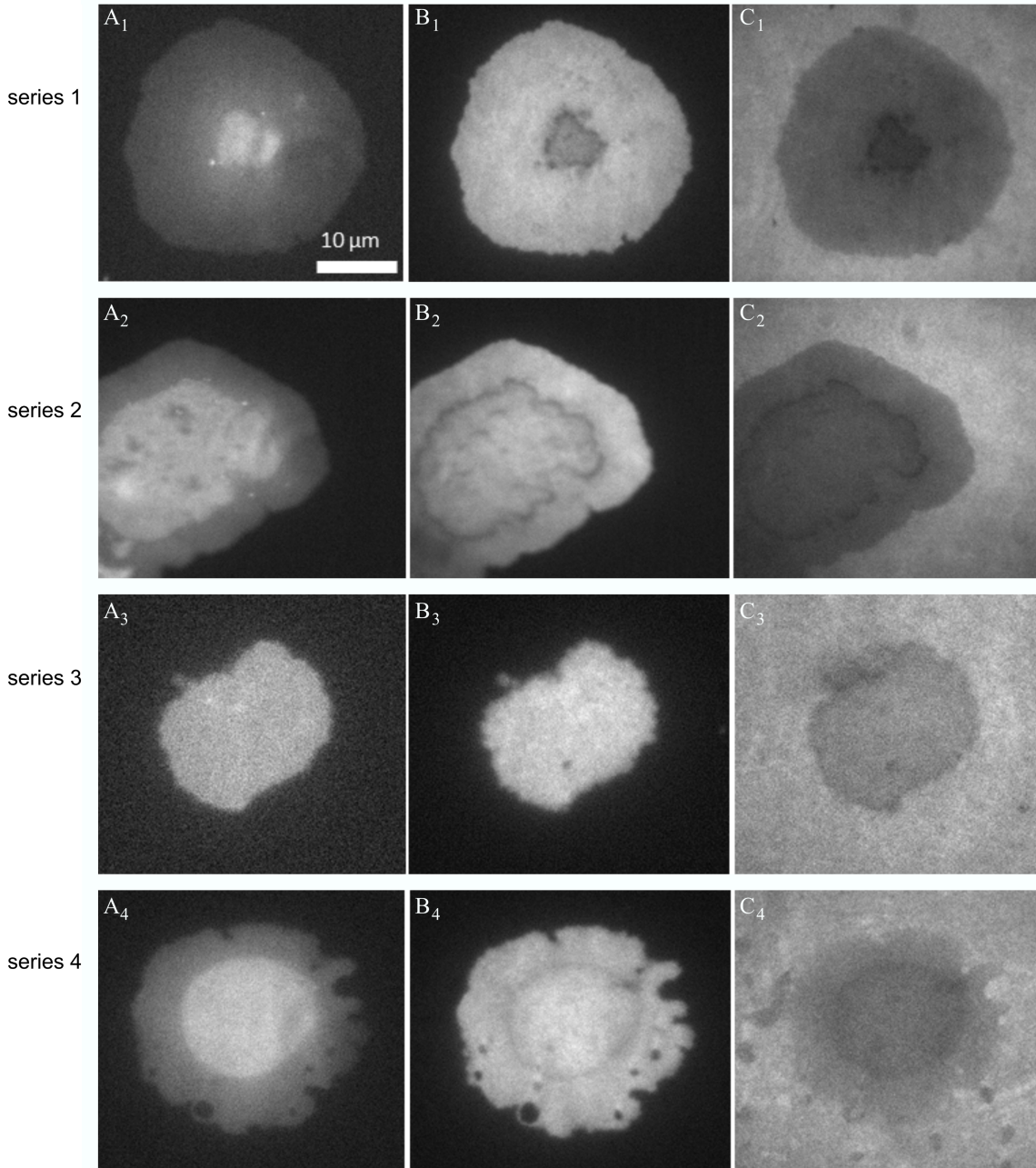


Figure 5: Images of supported lipid membrane for different concentration of NaOH (series 1 : $23 \mu\text{M}$, series 2 : $35 \mu\text{M}$, series 3 : $47 \mu\text{M}$, series 4 : $58 \mu\text{M}$) observed in TIRF illumination at 633 nm (A_i). Lipid bilayers are also excited at 457 nm and the emission of DiD (B_i) and the quenching of QDs layer (C_i) were collected with relevant band-pass filters.

the structure while only a single lipid bilayer is obtained at the periphery. At the junction of the bilayer and the quadrilayer, the QDs quenching is stronger which could be due to a decrease of the distance (Fig.5 C_2 , C_4). At the same time, the DiD emission in NEFM

images is lower due to a depletion of DiD during the formation of this structure (Fig.5 B₂, B₄). In the center, the DiD fluorescence recorded in NEFM seems to be not affected by the presence of the second bilayer. This clearly demonstrates that the second bilayer is out of the range of FRET process and its distance is greater than 10 nm from the center of the QDs layer. Indeed, the second bilayer is repelled by the first one, due to electrostatic repulsion as both bilayers were negatively charged. On the series 3, only a single bilayer is observed. On the series 1, the lipid organization in the center should be different than a simple stack of two lipid bilayer as the signal in NEFM decreases (Fig.5 B₁). This should be due to a depletion of DiD with a decrease of the distance. To avoid such artefacts related to multistack, we have analyzed zones where only one lipid bilayer is obtained (usually at the periphery of the structures). As previously, we have calculated from the quenching of QDs and according to the Equation 2, the ratio R/R_0 for several lysed vesicles (at least 10 vesicles for each sodium hydroxide concentration). Histograms of these distances are plotted in Fig.6. All histograms were fitted with a Gaussian model to get the mean value ($\langle R/R_0 \rangle$)

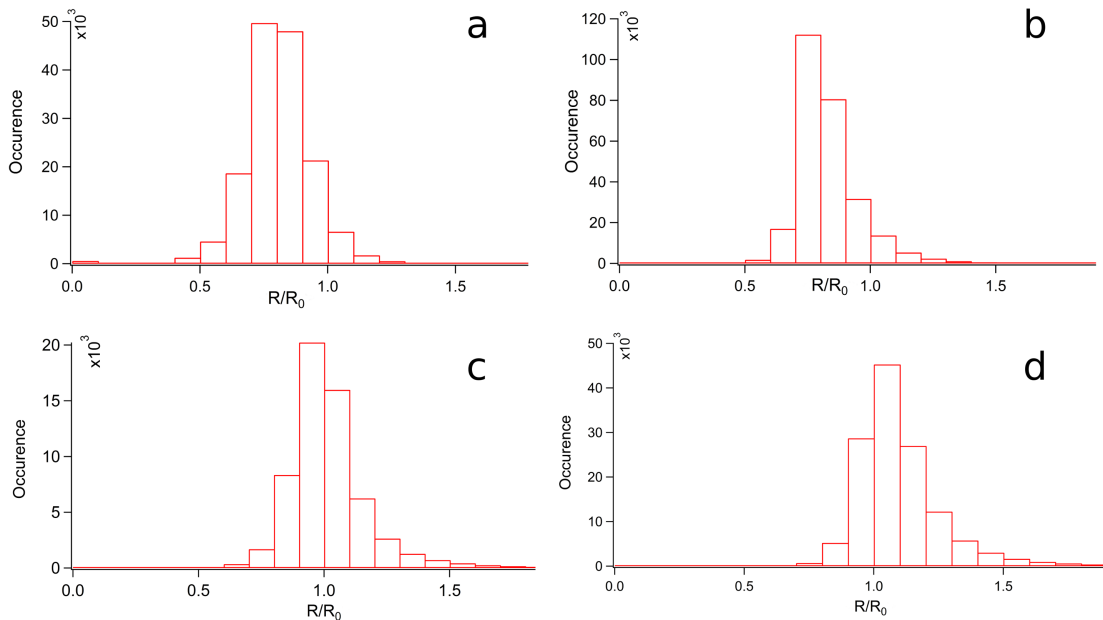


Figure 6: Histograms of R/R_0 distance obtained on at least ten vesicles at different NaOH concentrations (a: 23 μM , b: 35 μM , c : 47 μM and d : 58 μM).

and the standard deviation (σ). We observed clearly a shift to higher value when the NaOH

Table 2: Evolution of the spreading factor (S) measured with TIRFM and NEFM pictures as a function of the concentration of NaOH

[NaOH] ($\mu\text{mol/L}$)	S(TIRF)	S(NEFM)
87	0.66	0.23
116	0.50	0.13

concentration is increased. The water gap thickness increases with the salt concentration. Since $R_0 = 5.82 \text{ nm}$, we have plotted the evolution of $\langle d_0 \rangle$ as a function of the sodium hydroxide concentration (Fig.7). As the concentration increase, the interdistance d_0 from

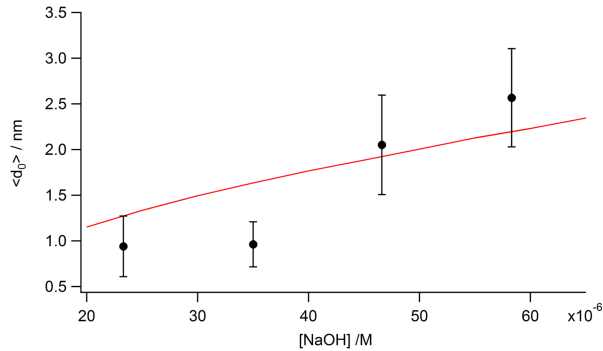


Figure 7: Variation of the average equilibrium inter distance d_0 , as function of salt concentration. In red, the equilibrium distance calculated from the simulations (see supporting informations).

the top of the QDs to the lipid membrane increases from 0.94 nm to 2.57 nm.

For salt concentration between 87 μM and 120 μM , we observed vesicles in adhesion without any lysis (Fig.S5). As previously proposed,¹⁷ we have estimated the apparent diameter (D) of GUVs in adhesion in this case. From TIRF and NEFM images we have measured a contact area, denoted C, and then calculated a spreading factor, denoted S, for both excitation cases ($S = C / (\pi(D/2)^2)$). As we can see in Table 2, S decreases as the salt concentration increases. Therefore, the mean equilibrium distance d_0 continues to increase as a function of the salt concentration. For salt concentrations higher than 120 μM , all vesicles are repelled far away from the surface and no fluorescence can be observed in NEFM imaging (S is lower than 0.1 as indicated by TIRF imaging). These results clearly indicate that the equilibrium distance d_0 between the membrane and the QDs continues to increase as a function of the

salt concentration.

To uncover which forces induce such behavior, we have performed simulations. In the case of GUVs lysis, we have to consider 3 forces: van der Waals attraction, electrostatic attraction and steric repulsion mediated by PLL and QDs ligands. These forces are detailed in the Supporting Information. For the electrostatic force, the surface potential and the potential of the lipid bilayer have been estimated. To characterize the potential of the functionalized glass coverslips, we measured the ζ -potential with a Zetasizer (Malvern, Nano-ZS) of micro-silica particles which exhibit the same surface functionalization with PLL. Note that the QDs are neutral and do not contribute to the effective charge of the surface. The ζ -potential was measured as a function of the salt concentration. We obtained that the ζ -potential is positive when the concentration of NaOH is lower than a threshold value and becomes negative for higher values of the salt concentration (Fig.S₃). More we add salt and more the positive charges on the PLL are screened and therefore the surface potential decrease. This decrease was modeled by using the Graham equation (see supporting information) and therefore the surface potential was calculated as a function of the salt concentration (Table S₁). We have also measured the ζ -potential of the lipid bilayer on Small Unilamellar Vesicles (SUVs). Their potential appears to be always negative and its value is around -25 mV. From all this data, one can calculate, for a given salt concentration the evolution of the potential energy of membrane/substrate interactions resulting from these three forces as a function of the distance between the surface and the lipid bilayer (Fig.S₇). The equilibrium distance d_0 can be easily deduced, as the minimum of the potential energy. This was done for various salt concentrations and d_0 was plotted together with our experimental data (Fig.7). We obtained a relative good agreement between this model and our experimental results. In both cases an increase of ≈ 1 nm of the equilibrium distance is achieved. The small jump observed in the experimental data points could be due to an abrupt increase in the gyration radius of repeller molecules when the salt concentration increases (only a gradual increase is taking into account in the simulations).

In the case where no lysis of vesicles was observed, two more forces must be considered. The first one is the gravitational attraction as vesicles have sucrose inside and are suspended in glucose solution. The difference of density between sucrose and glucose induce the sedimentation of vesicles. The expression of this attractive potential is given in the supporting information. The second force is the Helfrich repulsion and its expression is also given in supporting information. Lipid membranes fluctuated freely in bulk, but when GUVs are closed to a surface, the thermal fluctuation spectrum changed and it yielded to a repulsive force. We have showed, as previously observed¹⁷ that the equilibrium distance is about few hundreds nanometers (Fig.S₈), which is in good agreement with our experimental results.

Materials and Methods

Materials

CdSe/ZnS quantum dots (748099), (3-mercaptopropyl)trimethoxysilane (175617), poly-L-lysine solution (P4707) and DOPC (1,2-Dioleoyl-sn-glycero-3-phosphocholine, P6354) were purchased from Sigma-Aldrich. DiD (DiC18(5)-DS (1,1'-Dioctadecyl-3,3,3,3'-Tetramethyl-indodicarbocyanine-5,5'-Disulfonic Acid, D12730) was purchased from ThermoFisher Scientific. Thickness-corrected glass coverslip (170 μm +/- 10 μm) were purchased from Assistant, Sondheim, Germany.

Giant Unilamellar Vesicles (GUVs) preparation

GUVs were prepared using the standard electroformation method. We mixed DOPC (2 mg/mL in methanol/chloroform (9:1)) with DiD (18 μM in methanol /chloroform). The lipid membrane is negatively charged due to the presence of two benzene sulfonic acid groups on DiD. 50 μL of the mixture is deposited on two ITO (Indium Tin Oxide) conducting plates. After evaporation of the solvent in a vacuum chamber, the plates were fixed face to face in a teflon holders in order to make a hermetic chamber. A 200 mM sucrose solution at pH 6

was injected to hydrate lipids. Then an alternative electric field was applied between the two ITO plates at 10 Hz. The electric field intensity was increased from 0.2 V to 0.8 V and maintained overnight. Later, the electric field was decreased to 0.2 V at 4 Hz for 20 minutes. Then, GUVs were gently removed from the ITO plates with a thick needle syringe (18G) to avoid lysis.

Surface preparation

Prior to any chemical treatment, glass coverslips were cleaned by immersion in a Piranha Solution (50 % H_2SO_4 , 50% H_2O_2) for 30 minutes and rinsed extensively with pure water. S1813 photoresist was added between two coverslips to cover one side of coverslips, leaving the other side free for the silanization. Then, this new structure was incubated in the (3-mercaptopropyl)trimethoxysilane diluted in anhydrous toluene at 0.01 % for 12 hours. Afterwards, the substrate was immersed in a solution of quantum dots (QDs) in toluene (0.08 mg/L) for 24 hours. At last, the substrate is rinsed with toluene and next with acetone in order to remove the S1813 photoresist. At the end, one can obtain 2 functionalized coverslips with QDs on one side. All reactions were performed in a glove box under argon gas. Then the coverslips were incubated for 60 min in a poly-L-lysine solution (0.01 % w/v).

Microscopy

Our set-up was extensively described in a previous paper.²⁰ Briefly, two laser beams were implemented (one at 457 nm for QDs excitation, and one at 633 nm for DiD excitation). A 100 x Zeiss objective (plan-achromat, NA= 1.46) was used to create a widefield illumination. A rotatable mirror was mount to switch between Total Internal Reflection Fluorescence (TIRF) and epi-illumination. Band-pass filters (Semrock FF01-600/14 and Semrock FF01-682/14) were added to observe the QDs emission (the spectrum window is 593 nm-607nm) or the DiD emission (spectrum window is 670-694 nm). The camera used in all experiments was a CoolSNAP HQ2 (Photometrics Scientific).

Conclusion

We have studied adhesion of vesicles using non-radiative excitation fluorescence microscopy (NEFM). This original approach is based on a FRET process between a surface coated with a monolayer of QDs and fluorescence probes present in the sample. From the quenching of the QDs, the interdistance between the surface and the membrane was assessed for different adhesion strength. The high sensitivity of FRET allows us to determine variation of the equilibrium distance with ≈ 1 nm precision along the optical axis. Compared to other super-resolution techniques like STORM,²⁵⁻²⁷ PALM,²⁸ STED²⁴ or MIET,^{29,41} NEFM does not need long time acquisition, complex data processing or high laser power. Samples can therefore be illuminated for a long time with a negligible photobleaching. Moreover this technique can be easily implemented on any kind of inverted microscopes. Then, dynamical aspects of cell adhesion and migration can be studied as the acquisition time is typically few hundreds ms. NEFM is also relevant to study the interaction and diffusion of supported lipid bilayers on nanoroughness surfaces.⁴² Finally, this method is also well suited to study biological samples as it was previously demonstrated.¹⁹ We believe that our technique can be used to probe the dynamic of focal adhesions and also localize precisely cell integrins involved in the focal adhesion plaques.

Acknowledgement

This work was supported in part by the Grand Troyes, the Conseil départemental de l'Aube, the Fond Européen de Développement Régional (CELLnanoFLUO project).

Supporting Information Available

The following files are available free of charge. We provide further details on lifetime measurements of QDs, the justification on the FRET law used, the determination of the surface

potential, the FRET evidence, the adhesion of GUVs, the expression of the different forces involved in the surface/membrane interactions and the total interaction potential in case of strong interaction or in case of electrostatic repulsion.

Author Contributions

L. R. designed the NEFM setup, performed experiments and data analysis. D. E. A performed measurements on the determination of surface potential. R. J. designed the NEFM setup, supervised experiments, performed lifetime measurements and developed the theory. C. V. performed and supervised experiments and developed the data processing routine.

References

- (1) Kalinin, S.; Peulen, T.; Sindbert, S.; Rothwell, P. J.; Berger, S.; Restle, T.; Goody, R. S.; Gohlke, H.; Seidel, C. A. A toolkit and benchmark study for FRET-restrained high-precision structural modeling. *Nat. Methods* **2012**, *9*, 1218–1225.
- (2) Miyawaki, A.; Llopis, J.; Heim, R.; McCaffery, J. M.; Adams, J. A.; Ikura, M.; Tsien, R. Y. Fluorescent indicators for Ca²⁺-based on green fluorescent proteins and calmodulin. *Nature* **1997**, *388*, 882–887.
- (3) Hildebrandt, N.; Spillmann, C. M.; Algar, W. R.; Pons, T.; Stewart, M. H.; Oh, E.; Susumu, K.; Díaz, S. A.; Delehanty, J. B.; Medintz, I. L. Energy Transfer with Semiconductor Quantum Dot Bioconjugates: A Versatile Platform for Biosensing, Energy Harvesting, and Other Developing Applications. *Chemical Reviews* **2017**, *117*, 536–711.
- (4) Hodgson, L.; Spiering, D.; Sabouri-Ghomi, M.; Dagliyan, O.; DerMardirossian, C.; Danuser, G.; Hahn, K. M. FRET binding antenna reports spatiotemporal dynamics of GDI-Cdc42 GTPase interactions. *Nature Chemical Biology* **2016**, *12*, 802–809.

- (5) Kaizuka, Y.; Groves, J. T. Structure and Dynamics of Supported Intermembrane Junctions. *Biophys. J.* **2004**, *86*, 905–912.
- (6) Limozin, L.; Sengupta, K. Modulation of vesicle adhesion and spreading kinetics by hyaluronan cushions. *Biophys. J.* **2007**, *93*, 3300–3313.
- (7) Vézy, C.; Massiera, G.; Viallat, A. Adhesion induced non-planar and asynchronous flow of a giant vesicle membrane in an external shear flow. *Soft Matter* **2007**, *3*, 844–851.
- (8) Dos Santos, M. C.; Détureche, R.; Vézy, C.; Jaffiol, R. Axial nanoscale localization by normalized total internal reflection fluorescence microscopy. *Opt. Lett.* **2014**, *39*, 869–872.
- (9) Huang, Z.-H.; Massiera, G.; Limozin, L.; Boullanger, P.; Valignat, M.-P.; Viallat, A. Sensitive detection of ultra-weak adhesion states of vesicles by interferometric microscopy. *Soft Matter* **2010**, *6*, 1948–1957.
- (10) Zilker, A.; Engelhardt, H.; Sackmann, E., Dynamic reflection interference contrast (RIC-) microscopy : a new method to study surface excitations of cells and to measure membrane bending elastic moduli. *J. Phys. France* **1987**, *48*, 2139–2151.
- (11) Rädler, J.; Sackmann, E. Imaging optical thicknesses and separation distances of phospholipid vesicles at solid surfaces. *J. Phys. II* **1993**, *3*, 727–748.
- (12) Bereiter-Hahn, J.; Fox, C. H.; Thorell, B. Quantitative reflection contrast microscopy of living cells. *J. Cell Biol.* **1979**, *82*, 767–779.
- (13) Geiger, B.; Avnur, Z.; Kreis, T. E.; Schlessinger, J. In *The Cytoskeleton*; Shay, J. W., Ed.; Springer US: Boston, MA, 1984; pp 195–234.
- (14) Schilling, J.; Sengupta, K.; Goennenwein, S.; Bausch, A.; Sackmann, E. Absolute interfacial distance measurements by dual-wavelength reflection interference contrast microscopy. *Phys. Rev. E* **2004**, *69*, 1–9.

- (15) Braun, D.; Fromherz, P. Fluorescence interference-contrast microscopy of cell adhesion on oxidized silicon. *Appl. Phys. A Mater. Sci. Process.* **1997**, *65*, 341–348.
- (16) Kaizuka, Y.; Groves, J. T. Hydrodynamic damping of membrane thermal fluctuations near surfaces imaged by fluorescence interference microscopy. *Phys. Rev. Lett.* **2006**, *96*, 1–4.
- (17) Cardoso Dos Santos, M.; Vézy, C.; Jaffiol, R. Nanoscale characterization of vesicle adhesion by normalized total internal reflection fluorescence microscopy. *Biochim. Biophys. Acta - Biomembr.* **2016**, *1858*, 1244–1253.
- (18) Cardoso Dos Santos, M.; Détureche, R.; Vézy, C.; Jaffiol, R. Topography of Cells Revealed by Variable-Angle Total Internal Reflection Fluorescence Microscopy. *Biophys. J.* **2016**, *111*, 1316–1327.
- (19) Winckler, P.; Jaffiol, R.; Plain, J.; Royer, P. Nonradiative Excitation Fluorescence: Probing Volumes Down to the Attoliter Range. *J. Phys. Chem. Lett.* **2010**, *1*, 2451–2454.
- (20) Riachy, L.; Vézy, C.; Jaffiol, R. Non-radiative excitation fluorescence microscopy. *Proc.SPIE* **2016**, *9721*, 9721 – 9721 – 8.
- (21) Limozin, L.; Sengupta, K. Quantitative reflection interference contrast microscopy (RICM) in soft matter and cell adhesion. *ChemPhysChem* **2009**, *10*, 2752–2768.
- (22) Wong, A. P.; Groves, J. T. Molecular topography imaging by intermembrane fluorescence resonance energy transfer. *Proc. Natl. Acad. Sci. U. S. A.* **2002**, *99*, 14147–14152.
- (23) Weisenburger, S.; Boening, D.; Schomburg, B.; Giller, K.; Becker, S.; Griesinger, C.; Sandoghdar, V. Cryogenic optical localization provides 3D protein structure data with Angstrom resolution. *Nature Methods* **2017**, *14*, 141–144.

- (24) Hein, B.; Willig, K. I.; Hell, S. W. Stimulated emission depletion (STED) nanoscopy of a fluorescent protein-labeled organelle inside a living cell. *Proceedings of the National Academy of Sciences* **2008**, *105*, 14271–14276.
- (25) Bourg, N.; Mayet, C.; Dupuis, G.; Barroca, T.; Bon, P.; Lécart, S.; Lévêque-Fort, S. Direct optical nanoscopy with axially localized detection. *Nature Photonics* **2015**, *9*, 587–593.
- (26) Deschamps, J.; Mund, M.; Ries, J. 3D superresolution microscopy by supercritical angle detection. *Opt. Express* **2014**, *22*, 29081–29091.
- (27) Winterflood, C. M.; Ruckstuhl, T.; Verdes, D.; Seeger, S. Nanometer Axial Resolution by Three-Dimensional Supercritical Angle Fluorescence Microscopy. *Phys. Rev. Lett.* **2010**, *105*, 108103.
- (28) Kanchanawong, P.; Shtengel, G.; Pasapera, A. M.; Ramko, E. B.; Davidson, M. W.; Hess, H. F.; Waterman, C. M. Nanoscale architecture of integrin-based cell adhesions. *Nature* **2010**, *468*, 580–584.
- (29) Baronsky, T.; Ruhlandt, D.; Brückner, B. R.; Schäfer, J.; Karedla, N.; Isbaner, S.; Hähnel, D.; Gregor, I.; Enderlein, J.; Janshoff, A.; Chizhik, A. I. Cell-Substrate Dynamics of the Epithelial-to-Mesenchymal Transition. *Nano Letters* **2017**, *17*, 3320–3326.
- (30) Jasieniak, J.; Smith, L.; Embden, J. V.; Mulvaney, P.; Califano, M. Re-examination of the Size-Dependent Absorption Properties of CdSe Quantum Dots. **2009**, 19468–19474.
- (31) Strickler, S. J.; Berg, R. A. Relationship between Absorption Intensity and Fluorescence Lifetime of Molecules. *The Journal of Chemical Physics* **1962**, *37*, 814–822.
- (32) Gong, K.; Zeng, Y.; Kelley, D. F. Extinction coefficients, oscillator strengths, and radiative lifetimes of CdSe, CdTe, and CdTe/CdSe nanocrystals. *J. Phys. Chem. C* **2013**, *117*, 20268–20279.

- (33) Gong, K.; Martin, J. E.; Shea-Rohwer, L. E.; Lu, P.; Kelley, D. F. Radiative lifetimes of zincblende CdSe/CdS quantum dots. *J. Phys. Chem. C* **2015**, *119*, 2231–2238.
- (34) Aubret, A.; Pillonnet, A.; Houel, J.; Dujardin, C.; Kulzer, F. CdSe/ZnS quantum dots as sensors for the local refractive index. *Nanoscale* **2016**, *8*, 2317–2325.
- (35) Lukosz, W.; Kunz, R. E. Light emission by magnetic and electric dipoles close to a plane interface I Total radiated power. *J. Opt. Soc. Am.* **1977**, *67*, 1607.
- (36) Chizhik, A. I.; Gregor, I.; Enderlein, J. Quantum Yield Measurement in a Multicolor Chromophore Solution Using a Nanocavity. *Nano Letters* **2013**, *13*, 1348–1351.
- (37) Collot, M.; Kreder, R.; Tatarets, A. L.; Patsenker, L. D.; Mely, Y.; Klymchenko, A. S. Bright fluorogenic squaraines with tuned cell entry for selective imaging of plasma membrane vs. endoplasmic reticulum. *Chem. Commun.* **2015**, *51*, 17136–17139.
- (38) Dale, R.; Eisinger, J.; Blumberg, W. The orientational freedom of molecular probes. The orientation factor in intramolecular energy transfer. *Biophysical Journal* **1979**, *26*, 161 – 193.
- (39) Axelrod, D. Carbocyanine dye orientation in red cell membrane studied by microscopic fluorescence polarization. *Biophysical Journal* **1979**, *26*, 557 – 573.
- (40) Chittchang, M.; Salamat-Miller, N.; Alur, H. H.; Velde, D. G. V.; Mitra, A. K.; Johnston, T. P. Poly(L-lysine) as a model drug macromolecule with which to investigate secondary structure and microporous membrane transport, part 2: diffusion studies. *Journal of Pharmacy and Pharmacology* **2002**, *54*, 1497–1505.
- (41) Chizhik, A. I.; Rother, J.; Gregor, I.; Janshoff, A.; Enderlein, J. Metal-induced energy transfer for live cell nanoscopy. *Nature Photonics* **2014**, *8*, 124 –127.

- (42) Blachon, F.; Harb, F.; Munteanu, B.; Piednoir, A.; Fulcrand, R.; Charitat, T.; Fragneto, G.; Pierre-Louis, O.; Tinland, B.; Rieu, J.-P. Nanoroughness Strongly Impacts Lipid Mobility in Supported Membranes. *Langmuir* **2017**, *33*, 2444–2453.